

Unveiling potential candidates for rare-earth-free permanent magnet and magnetocaloric effect applications: a high throughput screening in Fe-N alloys

Qiang Gao ^{a,b,&,*}, Ergen Bao ^{b,&}, Ijaz Shahid ^b, Hui Ma ^b, Xing-Qiu Chen ^{b,*}

^a School of Science, Shenyang University of Technology, Shenyang 110870, China

^b Shenyang National Laboratory for Materials Science, Institute of Metal Research, Chinese Academy of Sciences, Shenyang, 110016, China

Abstract:

Based on high-throughput density functional theory calculations, we have found 49 ferromagnetic cases in $\text{Fe}_x\text{N}_{1-x}$ ($0 < x < 1$) compounds, focusing especially on permanent magnet and giant magnetocaloric effect applications. It is found that 15 compounds are potential permanent magnets with a magneto-crystalline anisotropy energy more than 1 MJ/m^3 , filling in the gap of application spectrum between high-performance and widely used permanents. Among the potential permanent magnets, Fe_2N can be classified as a hard magnet while the other 14 compounds can be classified as semi-hard magnets. According to the calculations of magnetic deformation proxy, 40 compounds are identified as potential giant magnetocaloric effect candidates. We suspect that Fe-N compounds provide fine opportunities for applications in both rare-earth free permanent magnets and magnetocaloric effect.

Keywords: Permanent magnet, Magneto-crystalline anisotropy energy, Saturation magnetization, Magnetocaloric effect

1. Introduction

Nowadays, the advanced information and green energy technologies are becoming much more important than ever before for providing us efficient and convenient life [1,2], with the fast-expanding requirement of hybrid-electric vehicles, robotics, wind turbines, and automation. The consumption of energy is becoming larger and larger, leading serious greenhouse gas emissions and chemical pollution to the environment [1,3,4]. In the field of information technology, more permanent magnets are required to design devices with desired rate of transformation, storage, and transmission speed [2,5,6]. The permanent magnet is the fundamental basis to realize environmentally friendly and high-performance energy and information devices. In applications, the excellent permanent magnet is eager to have a sizable coercivity, a remarkable saturation magnetization (M_S), and a significant high Curie temperature (at least above room temperature). The upper limit of the macroscopic coercivity is intrinsically determined by the microscopic magneto-crystalline anisotropy energy (MAE), which is associated with spin-orbit coupling (SOC) effect. At present, the commercially large scale applied permanent magnets are the rare-earth based compounds Sm-Co (MAE= 17 MJ/m^3 , $M_S=910 \text{ kA/m}$) and Nd-Fe-B (MAE= 5 MJ/m^3 , $M_S=720 \text{ kA/m}$) with a large energy density

[&] These authors contributed equally to this work and should be considered co-first authors.

^{*} Corresponding authors.

E-mail address: waveflying@163.com, lxygaoqiang@sut.edu.cn (Q. Gao); xingqiu.chen@imr.ac.cn (X.-Q. Chen).

$(BH)_{\max}$ [7]. Notably, the rare earth element is actually very rare and expensive, where the pollution problem also occurs during the production process. In commerce, the other widely used permanent magnets are transition metal-based compounds AlNiCo (MAE: 0.04 MJ/m³, M_S : 50 kA/m) and ferrites (MAE: 0.03 MJ/m³, M_S : 125 kA/m) with the relatively small energy density but cheaper cost [8]. Apparently, there is a remarkable gap in the application spectrum between such two types of commercial permanent magnets, waiting for the design of more permanent magnets with lower cost and reduced pollution. On the other hand, the realization of giant magnetocaloric effect (MCE) in magnets Gd₅Si₂Ge₂ [9] and LaFeSi₁₃ [10] has accelerated the studies and applications of high-efficiency refrigeration, playing an important role in green energy technology with environmentally friendly production process [11]. In this regard, it is a good chance to design rare-earth-free permanent magnets and giant magnetocaloric effect candidates with less cost to fill in the empty region of the application spectrum for advanced information and green energy devices [7,12].

The pristine α -Fe has a saturation magnetization as large as 217.6 emu/g (1710.34 emu/cm³) [13] at room temperature but suffers from a significantly weak magneto-crystalline anisotropy energy of 1.34 μ eV /Fe (0.036 MJ/m³) [14] due to the underlying cubic symmetry. To design rare-earth-free gap permanent magnets, the tetragonal distortion should be induced into the cubic Fe by means of alloy technology, substitutional and interstitial doping as well as imposed strain [15,16]. For example, DFT calculations predict that by alloying, the Fe-Co system achieves various tetragonal distortions with an enhanced MAE in the order of 700-800 eV/at. and a comparable magnetization ($\approx 1.6\sim 2.3\mu_B$ /at.) to the pristine α -Fe [17], which is validated by the following experiments by observing a MAE of 2.9 MJ/m³ with a magnetization of 2.5 μ_B /at. at 400 K in the Fe_{0.36}Co_{0.64}/Pt superlattices [18]. However, the tetragonal distortion of Fe-Co is relaxed when the thickness is larger than 2 nm, hindering the application [19]. Moreover, both theoretical and experimental studies have revealed that the tetragonal distortion in Fe-Co thin film can be stabilized by inducing interstitial dopants of carbon [20] and boron [21], where the MAE is as large as 0.5 MJ/m³ with a doped ratio of 4 at% for B [21]. Following this idea, the interstitial dopants (B, H, C, N) have been induced to cubic full Heusler compounds to design rare-earth-free gap permanent magnets by systematic high-throughput screening calculations, where 32 promising candidates fill in the application spectrum gap with a substantial out-of-plane uniaxial MAE (larger than 0.4 MJ/m³) [22]. High-throughput screening for MAB phase compounds predicts 23 rare-earth-free permanent magnets with a uniaxial MAE larger than 0.4 MJ/m³ and 99 promising MCE candidates with a magnetic deformation $\sum_M > 1.5\%$ [23]. Using RF magnetron sputtering technology, the α' -Fe₈N thin film is grown on the substrate of MgO [001] [24]. The saturation magnetization is observed to be about 1750 emu/cm³ with an uniaxial out-of-plane MAE of 0.775 meV/f.c. (6.0×10^6 erg/cm³), originating from the high susceptibility of Fe atoms surrounding the interstitial N based on theoretical calculations [24]. More recently, it is reported that a large quantity of powder of α' -Fe₈N can be produced at low temperatures by spark plasma sintering [25]. Apparently, carbonization, boronization, and nitrogenation reactions can induce a stable tetragonal distortion hence an enhanced MAE in α -Fe. Particularly, nitrogenation reaction tends to give rise to negative formation energies, meaning more iron-nitride compounds can be designed. Apart from permanent magnets, iron-nitride also has the potential to be applied in MCE applications. As reported in Ref. [26], the ϵ -Fe₃N and γ' -Fe₄N are potential good MCE materials due to their large magnetic deformation.

Motivated by the above, we have conducted a systematic high-throughput screening for Fe-N intermetallic compounds based on density functional theory (DFT) calculations, especially focusing

on the rare-earth-free permanent magnet and giant magnetocaloric applications. In our recent research paper [27], we have identified 49 ferromagnetic (FM) compounds with thermodynamic (convex hull smaller than 0.075 eV/at.), mechanical, and dynamical stabilities, focusing on the hardness. In this follow-up paper, we design the rare-earth-free permanent magnet and magnetocaloric applications based on the 49 stable magnetic $\text{Fe}_x\text{N}_{1-x}$ ($0 < x < 1$) alloys.

2. Computational details

As mentioned in our recent paper [28], the structures of the Fe-N candidates are obtained by the evolutionary algorithm from the USPEX 10.5.0 code (Universal Structure Prediction: Evolutionary Xtallography) [29–31]. The selected criteria for a structure are set as a negative formation energy, a convex hull smaller than 0.075 eV/at, mechanical (elastic constants) and dynamical (phonon spectral are calculated based on density functional perturbation theory by using Phonopy code [32,33]) stabilities. All calculations are performed by Vienna ab initio simulation package (VASP) based on density functional theory (DFT) using the projector augmented wave method [34,35] in the present research paper. The valence states are selected as $2s^22p^3$ and $3d^74s^1$ for N and Fe atoms. The cutoff energy for the plane wave is set to 500 (450) eV, and the energy convergence criterion is set to 1×10^{-7} (1×10^{-6}) eV with a k -space density of 50 (30) \AA^{-1} for MAE (structure relaxation) calculations.

3. Results and discussion

3.1 MAE

As known, magneto-crystalline anisotropy energy plays a fundamental role in the application of magnetic materials. As to permanent magnets, MAE is the atomic origination of the macroscopic coercivity. The broken continuous symmetry leads to energy dependence on the orientation of the spin in magnetic materials, *i.e.* MAE is expressed by

$$K_{\hat{n}_1-\hat{n}_2} = E_{\hat{n}_1} - E_{\hat{n}_2}, \quad (1)$$

where $E_{\hat{n}_{1/2}}$ denotes the energy for magnetization along the direction of $\hat{n}_{1/2}$. For a material with an arbitrary structure, the selected orientations are [001], [010], and [100], leading to three possible MAE values, namely $K_{100-001}$, $K_{001-010}$, and $K_{100-010}$. The distribution of maximum absolute MAE ($|K_{\max}|$) as a function of the square of saturation magnetization is shown in Fig. 1 for the Fe-N compounds, comparing with the experimentally realized permanent magnets [1,8,36]. Overall, the 49 FM compounds have filled in the empty region of the application spectral between MAE and MS. Notably, we have summarized 15 candidates with a sizable MAE (at least one MAE larger than 0.4 MJ/m^3) in Table A1, which are potential rare-earth-free gapped permanent magnets filling in the gap of application spectral between high-performance permanent magnets (*i.e.* FePd and CoPt₃) with underlying heavy element and widely used transition-metal based permanent magnet (AlNiCo and ferrites). In this point of view, the Fe-N compounds can spread the application range of permanent magnets.

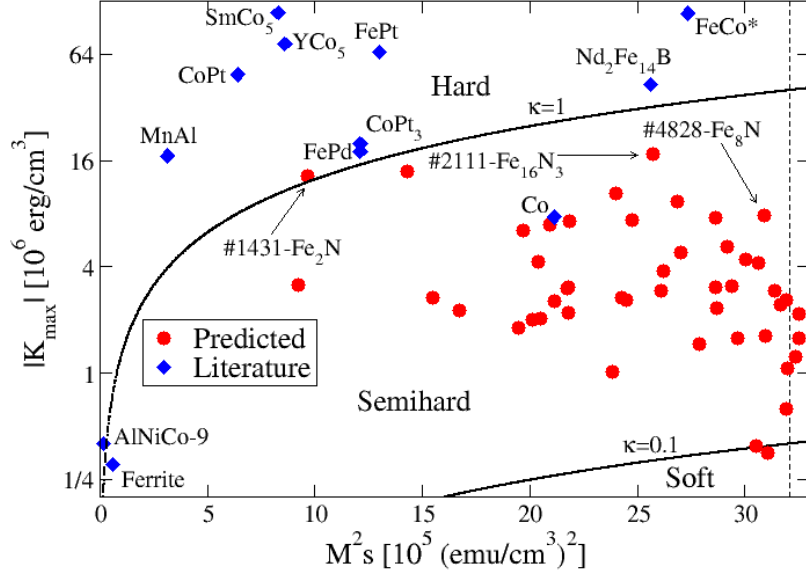


Fig. 1. The application spectrum of maximum absolute magneto-crystalline anisotropy (K_{\max}) vs. saturation magnetization (M_S) for ferromagnetic $\text{Fe}_x\text{N}_{1-x}$ ($0 < x < 1$) alloys. The filled blue diamond and red circle symbols represent the data sets of well-known permanent magnets and the predicted $\text{Fe}_x\text{N}_{1-x}$ ($0 < x < 1$) alloys, respectively. The solid black lines correspond to the magnetic hardness of the compounds given by $\kappa = \sqrt{K_1/(\mu_0 M_S)^2}$, where $\kappa > 1$, $0.1 < \kappa < 1$, and $\kappa < 0.1$ represent the hard, semi-hard, and soft regions. The dashed vertical line indicates that the magnitude of magnetization is equal to that of pure α -iron.

For validation, we have compared M_S and MAE with the associated data from references. For instance, α'' - Fe_8N (#4828) is also detected in our calculations with an out-of-plane MAE of 0.786 MJ/m^3 (0.786 $\text{meV}/\text{f.c.}$) and M_S of 1758.35 emu/cm^3 in our calculations. Such values can be well comparable with the experimentally observed saturation magnetization (about 1750 emu/cm^3) and calculated MAE (0.775 $\text{meV}/\text{f.c.}$ or 0.6 MJ/m^3) in Ref. [24]. For ϵ - Fe_3N (#1908), the M_S is 1419.12 emu/cm^3 (2.060 μ_B/Fe) with an in-plane MAE of 0.202 MJ/m^3 , where the density is 7.42 g/cm^3 based on Material Project [37]. The saturation magnetization can be compared with the experimental result of the ϵ - Fe_3N nanoparticles (1.5 μ_B/Fe , 1143 emu/cm^3) [38], while the MAE is roughly comparable with the result of the thin film ϵ - $\text{Fe}_{3.02}\text{N}$ (0.0326 MJ/m^3 , based on the coercivity $H_C = 207$ Oe at room temperature) [39]. The comparable data indicates the reliability of our calculations.

Among all the Fe-N alloys (including the newly predicted cases as well as α'' - Fe_8N and ϵ - Fe_3N), it is found that the triclinic Fe_{16}N_3 (#2111) compound has the largest out-of-plane MAE of 1.751 MJ/m^3 (0.139 meV/Fe) with also a remarkable high M_S of 1603.307 emu/cm^3 (1.850 μ_B/Fe). It is noticed that such MAE value is more than twice that of that of α'' - Fe_8N , and can be comparable with that of the well-known permanent magnets $L1_0$ -type MnAl ($K_u = 1.525$ MJ/m^3) [40] and FePd ($K_u = 1.8$ MJ/m^3) [41], while the M_S of Fe_{16}N_3 can even be comparable with that of the high-performance permanent magnet $\text{Nd}_2\text{Fe}_{14}\text{B}$ ($M_S = 1600$ emu/cm^3) [1,42]. Moreover, we also find three other candidates with a MAE larger than 1 MJ/m^3 but an in-plane magnetization, *i.e.* the hexagonal #6365- Fe_7N_3 (MAE = 1.384 MJ/m^3 , $M_S = 1195.632$ emu/cm^3), orthorhombic #1431- Fe_2N (MAE = 1.300

MJ/m³, $M_S=983.927$ emu/cm³), and orthorhombic #5076-Fe₄N (MAE=1.047 MJ/m³, $M_S=1548.482$ emu/cm³). Particularly, #1431-Fe₂N is a hard magnet because the dimensionless figure of merit $\kappa > 1$ ($\kappa = \sqrt{K_1/(\mu_0 M_S)^2}$) [43], which can be applied in various situations since the MAE is retained regardless of the manufacturing shape [2,36]. In addition, the other 14 predicted potential rare-earth-free gapped permanent magnets (in Table A1) are all semi-hard magnets due to $0.1 < \kappa < 1$, which are malleable and can be machined with standard metal-working tools [36,44].

Although with weak MAEs, the compounds #7124-Fe₂₀N (triclinic), #2879-Fe₁₆N (orthorhombic), #2518-Fe₁₉N (triclinic), #4467-Fe₁₅N (triclinic), #3110-Fe₁₄N (triclinic), and #1966-Fe₁₂N (monoclinic) respectively have significantly large saturation magnetizations of 1803.574 emu/cm³ (MAE=0.157 MJ/m³), 1802.684 emu/cm³ (MAE=0.216 MJ/m³), 1799.372 emu/cm³ (MAE=0.123 MJ/m³), 1788.767 emu/cm³ (MAE=0.106 MJ/m³), 1787.317 emu/cm³ (MAE=0.063 MJ/m³), and 1786.716 emu/cm³ (MAE=0.261 MJ/m³), which are larger than that of pure Fe (1784.761 emu/cm³, based on our DFT calculations). The distribution of M_S and the content ratio (x) of Fe is shown in Fig. 2 for Fe_xN_{1-x} ($0 < x < 1$) intermetallic compounds. Obviously, the saturation magnetization increases approximately linearly with the increasing of the content ratio of Fe. On the other hand, the different chemical environment can induce different magnitude of saturation magnetization for compounds with the same content ratio of Fe.

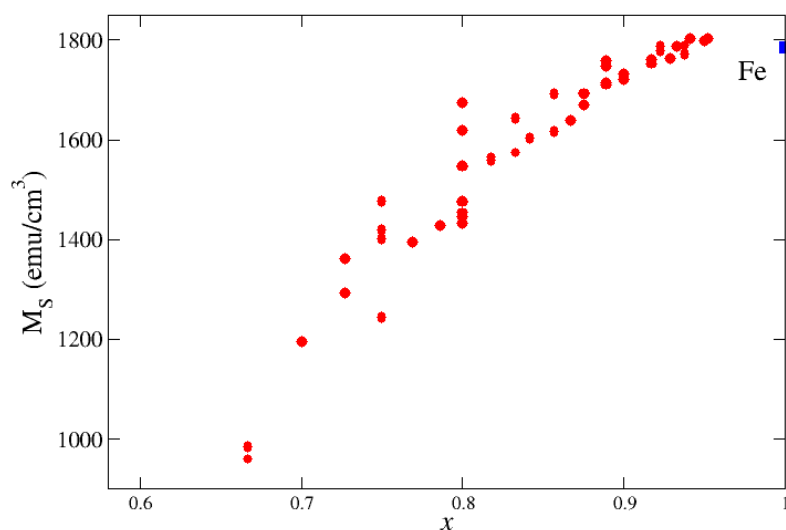


Fig. 2. The distribution of saturation magnetization (M_S) with respect to the content ratio x in Fe_xN_{1-x} ($0 < x < 1$) compounds. The red circle stands for the data set of the predicted compounds, while the blue square is the data of the pure α -iron.

3.2 MCE

Turning now to MCE applications, the potential fine MCE candidates can be easily screened by DFT calculations based on magnetic deformation (Σ_M) proxy, which is strongly associated with the essential parameter of entropy change ΔS_M for magneto-structural phase transition in MCE application [26]. The magnetic deformation is defined as a percentage indicator in terms of the degree of

the Lagrangian finite strain tensor of lattice deformation ($\boldsymbol{\eta}$)

$$\Sigma_M = \frac{1}{3} \sqrt{\eta_1^2 + \eta_2^2 + \eta_3^2} \times 100, \quad (2)$$

$$\boldsymbol{\eta} = \frac{1}{2} (\mathbf{P}^T \mathbf{P} - \mathbf{I}). \quad (3)$$

Here, $\mathbf{P} = \mathbf{A}_{\text{NM}}^{-1} \cdot \mathbf{A}_M$, where \mathbf{A}_{NM} (or \mathbf{A}_M) denotes the lattice constant in non-magnetic/magnetic structure. It is demonstrated that only with a magnetic deformation $\Sigma_M > 1.5\%$ can a compound be a potential MCE material [26].

We have found 40 newly potential MCE candidates ($\Sigma_M > 1.5\%$) among Fe-N alloys, where the relationship between saturation magnetization and magnetic deformation is shown in Fig. 3, also listing in Table A2. The magnetic deformation proxies for ϵ -Fe₃N (#1908) and γ' -Fe₄N (#2105) are respectively 1.93% and 1.92%, which are in good agreement with the results (1.88% and 1.93%) reported by Bocarsly *et al.* in Ref. [26]. Apparently, the correlation between M_S and Σ_M can be roughly regarded as positive in Fe-N alloys, which is similar to the relationship in MAB phase compounds [23]. Overall, we have found 41 compounds with a magnetic deformation $\Sigma_M > 1.5\%$, where 17 compounds even have the magnetic deformation larger than 7%. Particularly, it is found that the magnetic the deformation for the triclinic Fe₇N (#2952) is surprisingly as large as 9.36%. It is noted the magnetic deformation for pure α -Fe is 1.57%. Moreover, it is found that the most promising permanent magnets (MAE > 1 MJ/m³) #2111-Fe₁₆N₃, #6365-Fe₇N₃, #1431-Fe₂N, and #5076-Fe₄N are also potential MCE candidates, where the magnetic deformations are respectively 6.65%, 2.24%, 1.78%, and 4.69%. In this regard, such four compounds are promising candidates in both permanent magnet and giant magnetocaloric effect applications. All in all, we suspect that the Fe-N alloy system is a good playground to realize giant magnetocaloric effect applications.

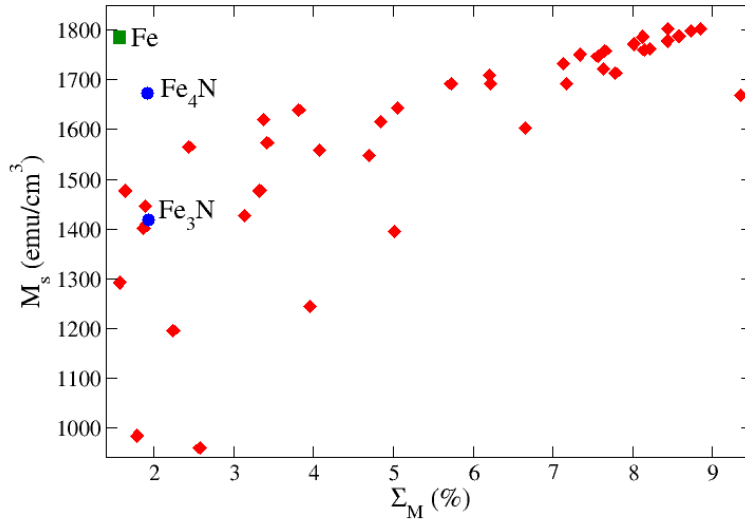


Fig. 3. The relationship between saturation magnetization (M_S) and magnetic deformation (Σ_M) for the 40 potential giant magnetocaloric effect candidates ($\Sigma_M > 1.5\%$), displayed by the red diamonds. The green square represents the data set of the pure α -Fe (based on our calculations), while the blue circles are the data points of ϵ -Fe₃N and γ' -Fe₄N.

4. Conclusions

In summary, we have carried out a systematic high-throughput DFT screening for permanent magnets and giant magnetocaloric effect candidates in $\text{Fe}_x\text{N}_{1-x}$ ($0 < x < 1$) intermetallic compounds. In total, 49 ferromagnetic compounds are identified in the Fe-N system. It is found that 15 compounds are potential permanent magnets with a magneto-crystalline anisotropy energy larger than 0.4 MJ/m^3 , where Fe_2N is a hard magnet while the other 14 candidates are semi-hard magnets. Such predicted permanent magnets can be applied as rare-earth-free gapped permanent magnets, spreading the application spectrum. Particularly, there are four promising permanent magnet candidates with a MAE more than 1 MJ/m^3 . The saturation magnetization and the content ratio x of Fe behaves like an approximate linear relationship in $\text{Fe}_x\text{N}_{1-x}$ ($0 < x < 1$). Based on the magnetic deformation proxy, 40 newly potential giant magnetocaloric effect candidates are discovered among $\text{Fe}_x\text{N}_{1-x}$ ($0 < x < 1$) compounds, where the magnetic deformation of Fe_7N is significantly large as 9.36%. The $\text{Fe}_x\text{N}_{1-x}$ compound is a fine playground to design permanent magnets and giant magnetocaloric effect applications.

CRedit authorship contribution statement

Qiang Gao: Conceptualization, Data curation, Formal analysis, Investigation, Methodology, Validation, Visualization, Writing – original draft, Writing – review and editing, **Ergen Bao:** Data curation, Formal analysis, Investigation, Validation, **Ijaz Shahid:** Data curation, Formal analysis, **Hui Ma:** Conceptualization, Formal analysis, Investigation, Methodology, Project administration, Writing – review and editing, **Xing-Qiu Chen:** Funding acquisition, Project administration, Software, Supervision, Writing – review and editing.

Declaration of Competing Interest

The authors declare that they have no known competing financial interests or personal relationships that could have appeared to influence the work reported in this paper.

Data availability

The structural ‘POSCAR’ for each compound is listed in the supplementary material with job id in the first line. The data that support the findings of this study are available from the corresponding author upon request.

Acknowledgements

This work was supported by National Science and Technology Major Project of China (No. J2019-VI-0019-0134), Liaoning Provincial Natural Science Foundation Project of China (No. 2023-MS-017) and National Natural Science Foundation of China (No. 52188101).

References

- [1] O. Gutfleisch, M.A. Willard, E. Brück, C.H. Chen, S.G. Sankar, J.P. Liu, *Magnetic Materials and Devices for the 21st Century: Stronger, Lighter, and More Energy Efficient*, *Advanced Materials* 23 (2011) 821–842. <https://doi.org/10.1002/adma.201002180>.
- [2] J.M.D. Coey, *Magnetism and Magnetic Materials*, Cambridge University Press, 2010.
- [3] S.A. Montzka, E.J. Dlugokencky, J.H. Butler, Non-CO₂ greenhouse gases and climate change, *Nature* 476 (2011) 43–50. <https://doi.org/10.1038/nature10322>.
- [4] V. Ramanathan, Y. Feng, Air pollution, greenhouse gases and climate change: Global and regional perspectives, *Atmospheric Environment* 43 (2009) 37–50. <https://doi.org/10.1016/j.atmosenv.2008.09.063>.
- [5] J.M.D. Coey, *Hard Magnetic Materials: A Perspective*, *IEEE Transactions on Magnetics* 47 (2011) 4671–4681. <https://doi.org/10.1109/TMAG.2011.2166975>.
- [6] J.M.D. Coey, *Perspective and Prospects for Rare Earth Permanent Magnets*, *Engineering* 6 (2020) 119–131. <https://doi.org/10.1016/j.eng.2018.11.034>.
- [7] J.M.D. Coey, *Permanent magnets: Plugging the gap*, *Scripta Materialia* 67 (2012) 524–529. <https://doi.org/10.1016/j.scriptamat.2012.04.036>.
- [8] K.-H. Müller, S. Sawatzki, R. Gauß, O. Gutfleisch, *Permanent Magnet Materials and Applications*, in: J.M.D. Coey, S.S.P. Parkin (Eds.), *Handbook of Magnetism and Magnetic Materials*, Springer International Publishing, Cham, 2021: pp. 1369–1433. https://doi.org/10.1007/978-3-030-63210-6_29.
- [9] V.K. Pecharsky, K.A. Gschneidner, Jr., *Giant Magnetocaloric Effect in Gd₅(Si₂Ge₂)*, *Physical Review Letters* 78 (1997) 4494–4497. <https://doi.org/10.1103/PhysRevLett.78.4494>.
- [10] O. Gutfleisch, A. Yan, K.-H. Müller, *Large magnetocaloric effect in melt-spun LaFe_{13-x}Si_x*, *Journal of Applied Physics* 97 (2005) 10M305. <https://doi.org/10.1063/1.1847871>.
- [11] J. Liu, T. Gottschall, K.P. Skokov, J.D. Moore, O. Gutfleisch, *Giant magnetocaloric effect driven by structural transitions*, *Nature Mater* 11 (2012) 620–626. <https://doi.org/10.1038/nmat3334>.
- [12] J. Cui, M. Kramer, L. Zhou, F. Liu, A. Gabay, G. Hadjipanayis, B. Balasubramanian, D. Sellmyer, *Current progress and future challenges in rare-earth-free permanent magnets*, *Acta Materialia* 158 (2018) 118–137. <https://doi.org/10.1016/j.actamat.2018.07.049>.
- [13] J. Crangle, G.M. Goodman, *The Magnetization of Pure Iron and Nickel*, *Proceedings of the Royal Society of London. Series A, Mathematical and Physical Sciences* 321 (1971) 477–491. <https://www.jstor.org/stable/77809> (accessed November 20, 2024).
- [14] J. Kübler, *Theory of Itinerant Electron Magnetism*, OUP Oxford, 2000.
- [15] Q. Gao, *High-throughput screening of multifunctional magnetic materials*, Ph.D. Thesis, Technische Universität Darmstadt, 2020. <https://doi.org/10.25534/tuprints-00014194>.
- [16] *High-throughput design of magnetic materials - IOPscience*, (n.d.). <https://iopscience.iop.org/article/10.1088/2516-1075/abbb25&title=iopscience.iop.org> (accessed November 20, 2024).
- [17] T. Burkert, L. Nordström, O. Eriksson, O. Heinonen, *Giant Magnetic Anisotropy in Tetragonal FeCo Alloys*, *Phys. Rev. Lett.* 93 (2004) 027203. <https://doi.org/10.1103/PhysRevLett.93.027203>.
- [18] G. Andersson, T. Burkert, P. Warnicke, M. Björck, B. Sanyal, C. Chacon, C. Zlotea, L. Nordström, P. Nordblad, O. Eriksson, *Perpendicular Magnetocrystalline Anisotropy in Tetragonally Distorted Fe-Co Alloys*, *Phys. Rev. Lett.* 96 (2006) 037205.

<https://doi.org/10.1103/PhysRevLett.96.037205>.

- [19] F. Yildiz, M. Przybylski, X.-D. Ma, J. Kirschner, Strong perpendicular anisotropy in $\text{Fe}_x\text{Co}_{1-x}$ alloy films epitaxially grown on mismatching Pd(001), Ir(001), and Rh(001) substrates, *Phys. Rev. B* 80 (2009) 064415. <https://doi.org/10.1103/PhysRevB.80.064415>.
- [20] L. Reichel, L. Schultz, S. Fähler, Lattice relaxation studies in strained epitaxial Fe-Co-C films, *Journal of Applied Physics* 117 (2015) 17C712. <https://doi.org/10.1063/1.4908031>.
- [21] L. Reichel, L. Schultz, D. Pohl, S. Oswald, S. Fähler, M. Werwiński, A. Edström, E.K. Delczeg-Czirjak, J. Rusz, From soft to hard magnetic Fe-Co-B by spontaneous strain: a combined first principles and thin film study, *J Phys Condens Matter* 27 (2015) 476002. <https://doi.org/10.1088/0953-8984/27/47/476002>.
- [22] Designing rare-earth free permanent magnets in heusler alloys via interstitial doping, *Acta Materialia* 186 (2020) 355–362. <https://doi.org/10.1016/j.actamat.2019.12.049>.
- [23] C. Shen, Q. Gao, N.M. Fortunato, H.K. Singh, I. Opahle, O. Gutfleisch, H. Zhang, Designing of magnetic MAB phases for energy applications, *J. Mater. Chem. A* 9 (2021) 8805–8813. <https://doi.org/10.1039/D0TA11026D>.
- [24] H. Zhang, I. Dirba, T. Helbig, L. Alff, O. Gutfleisch, Engineering perpendicular magnetic anisotropy in Fe via interstitial nitrogenation: N_{Fe} , *APL Materials* 4 (2016) 116104. <https://doi.org/10.1063/1.4967285>.
- [25] T. Saito, H. Yamamoto, D. Nishio-Hamane, Production of Rare-Earth-Free Iron Nitride Magnets (α -Fe₁₆N₂), *Metals* 14 (2024) 734. <https://doi.org/10.3390/met14060734>.
- [26] J.D. Bocarsly, E.E. Levin, C.A.C. Garcia, K. Schwennicke, S.D. Wilson, R. Seshadri, A Simple Computational Proxy for Screening Magnetocaloric Compounds, *ACS Publications* (2017). <https://doi.org/10.1021/acs.chemmater.6b04729>.
- [27] E. Bao, J. Zhao, Q. Gao, I. Shahid, H. Ma, Y. Luo, P. Liu, Y. Sun, X.-Q. Chen, The Fe-N system: crystal structure prediction, phase stability, and mechanical properties, (2024). <https://doi.org/10.48550/arXiv.2411.17193>.
- [28] E. Bao, J. Zhao, Q. Gao, I. Shahid, H. Ma, Y. Luo, P. Liu, Y. Sun, X.-Q. Chen, The Fe-N System: Crystal Structure Prediction, Phase Stability, and Mechanical Properties, (2024). <https://doi.org/10.2139/ssrn.5020769>.
- [29] A.O. Lyakhov, A.R. Oganov, H.T. Stokes, Q. Zhu, New developments in evolutionary structure prediction algorithm USPEX, *Computer Physics Communications* 184 (2013) 1172–1182. <https://doi.org/10.1016/j.cpc.2012.12.009>.
- [30] C.W. Glass, A.R. Oganov, N. Hansen, USPEX—Evolutionary crystal structure prediction, *Computer Physics Communications* 175 (2006) 713–720. <https://doi.org/10.1016/j.cpc.2006.07.020>.
- [31] A.R. Oganov, A.O. Lyakhov, M. Valle, How Evolutionary Crystal Structure Prediction Works—and Why, *Acc. Chem. Res.* 44 (2011) 227–237. <https://doi.org/10.1021/ar1001318>.
- [32] A. Togo, L. Chaput, T. Tadano, I. Tanaka, Implementation strategies in phonopy and phono3py, *J. Phys.: Condens. Matter* 35 (2023) 353001. <https://doi.org/10.1088/1361-648X/acd831>.
- [33] A. Togo, First-principles Phonon Calculations with Phonopy and Phono3py, *J. Phys. Soc. Jpn.* 92 (2023) 012001. <https://doi.org/10.7566/JPSJ.92.012001>.
- [34] G. Kresse, J. Furthmüller, Efficient iterative schemes for ab initio total-energy calculations using a plane-wave basis set, *Phys Rev B Condens Matter* 54 (1996) 11169–11186.

<https://doi.org/10.1103/physrevb.54.11169>.

- [35] G. Kresse, D. Joubert, From ultrasoft pseudopotentials to the projector augmented-wave method, *Physical Review B* 59 (1999) 1758–1775. <https://doi.org/10.1103/PhysRevB.59.1758>.
- [36] J. Mohapatra, X. Liu, P. Joshi, J.P. Liu, Hard and semi-hard Fe-based magnetic materials, *Journal of Alloys and Compounds* 955 (2023) 170258. <https://doi.org/10.1016/j.jallcom.2023.170258>.
- [37] A. Jain, S.P. Ong, G. Hautier, W. Chen, W.D. Richards, S. Dacek, S. Cholia, D. Gunter, D. Skinner, G. Ceder, K.A. Persson, Commentary: The Materials Project: A materials genome approach to accelerating materials innovation, *APL Materials* 1 (2013) 011002. <https://doi.org/10.1063/1.4812323>.
- [38] A.-M. Zieschang, J.D. Bocarsly, M. Dürrschnabel, L. Molina-Luna, H.-J. Kleebe, R. Seshadri, B. Albert, Nanoscale Iron Nitride, ϵ -Fe₃N: Preparation from Liquid Ammonia and Magnetic Properties, *Chem. Mater.* 29 (2017) 621–628. <https://doi.org/10.1021/acs.chemmater.6b04088>.
- [39] K. Oda, T. Yoshio, K. Oda, Preparation of Fe-N films by r.f. sputtering, *J Mater Sci* 25 (1990) 2557–2561. <https://doi.org/10.1007/BF00638058>.
- [40] J.H. Park, Y.K. Hong, S. Bae, J.J. Lee, J. Jalli, G.S. Abo, N. Neveu, S.G. Kim, C.J. Choi, J.G. Lee, Saturation magnetization and crystalline anisotropy calculations for MnAl permanent magnet, *Journal of Applied Physics* 107 (2010) 09A731. <https://doi.org/10.1063/1.3337640>.
- [41] H. Shima, K. Oikawa, A. Fujita, K. Fukamichi, K. Ishida, A. Sakuma, Lattice axial ratio and large uniaxial magnetocrystalline anisotropy in L1₀-type FePd single crystals prepared under compressive stress, *Phys. Rev. B* 70 (2004) 224408. <https://doi.org/10.1103/PhysRevB.70.224408>.
- [42] J. Cui, M. Kramer, L. Zhou, F. Liu, A. Gabay, G. Hadjipanayis, B. Balasubramanian, D. Sellmyer, Current progress and future challenges in rare-earth-free permanent magnets, *Acta Materialia* 158 (2018) 118–137. <https://doi.org/10.1016/j.actamat.2018.07.049>.
- [43] J.M.D. Coey, New permanent magnets; manganese compounds, *J. Phys.: Condens. Matter* 26 (2014) 064211. <https://doi.org/10.1088/0953-8984/26/6/064211>.
- [44] L. Yin, R. Juneja, L. Lindsay, T. Pandey, D.S. Parker, Semihard Iron-Based Permanent-Magnet Materials, *Phys. Rev. Appl.* 15 (2021) 024012. <https://doi.org/10.1103/PhysRevApplied.15.024012>.

Appendix A. Summaries of predicted permanent magnets and potential giant magnetocaloric effect candidates in $\text{Fe}_x\text{N}_{1-x}$ Compounds.

Table A1: The basic information for the predicted most promising permanent magnets (MAE larger than 0.4 MJ/m^3) in $\text{Fe}_x\text{N}_{1-x}$ ($0 < x < 1$) compounds. ID represents the job ID given by USPEX code. Com., ST, and SG denote the abbreviations of compound formula, structure type, and space group. In the ST column, TRI, HEX, ORT, MON, TET, and CUB mark the triclinic, hexagonal, orthorhombic, monoclinic, tetragonal and cubic crystal structure, respectively. ΔE_f and ΔE_H represent the formation and convex hull both in the unit of eV/at. MAE is the magneto-crystalline anisotropy energy in units of MJ/m^3 and meV/Fe . M_S is the saturation magnetization in units of emu/cm^3 and μ_B/Fe . The data (in bold font) of #4828- Fe_8N (α - Fe_8N) and #1908- Fe_3N (ϵ - Fe_3N) are also listed for comparison with references. The formation and convex hull can be checked in our recent paper [27].

ID	Com.	ST	SG	ΔE_f	ΔE_H	MAE	Easy-axis	M_S
2111	Fe_{16}N_3	TRI	$P\bar{1}$	-0.0004	0.0464	1.7509 (0.1389)	z	1603.307 (1.850)
6365	Fe_7N_3	HEX	$P6_3$	-0.0452	0.041	1.3840 (0.1193)	y	1195.632 (1.247)
1431	Fe_2N	ORT	$Pbcn$	-0.0431	0.0511	1.2995 (0.1138)	x	983.9266 (0.992)
5076	Fe_4N	ORT	$Cmcm$	-0.0073	0.0519	1.0470 (0.0852)	x	1548.482 (1.742)
2958	Fe_{13}N_2	MON	$C2$	-0.0002	0.0393	0.9369 (0.0736)	y	1639.209 (1.928)
2421	Fe_7N	MON	$C2/m$	-0.0122	0.0248	0.7536 (0.0590)	x	1691.75 (2.003)
1609	Fe_5N	MON	$C2$	-0.0077	0.0416	0.7376 (0.0591)	y	1573.671 (1.815)
840	Fe_3N	MON	$C2/m$	-0.0176	0.0564	0.7283 (0.0619)	z	1477.306 (1.628)
2018	Fe_4N	ORT	$Pmna$	-0.0313	0.0279	0.6929 (0.0559)	z	1445.983 (1.611)
1546	Fe_3N	ORT	$Immm$	-0.0088	0.0653	0.6385 (0.0535)	y	1402.264 (1.523)
8109	Fe_8N	TRI	$P1$	-0.0166	0.0163	0.5201 (0.0403)	z	1708.572 (2.034)
617	Fe_5N	MON	$C2/m$	-0.0069	0.0424	0.4829 (0.0388)	y	1643.37 (1.903)
1266	Fe_9N	MON	$C2/m$	-0.0157	0.0139	0.4432 (0.0341)	z	1732.425 (2.070)
7844	Fe_{11}N_3	TRI	$P\bar{1}$	-0.0003	0.0632	0.4246 (0.0343)	x	1427.379 (1.647)
3913	Fe_{11}N	MON	$C2/m$	-0.011	0.0137	0.4234 (0.0322)	z	1750.894 (2.106)
4828	Fe_8N	TET	$I4/mmm$	-0.0289	0.0040	0.7856 (0.0614)	z	1758.348 (2.111)
1908	Fe_3N	HEX	$P6_322$	-0.0740	0.0000	0.2021 (0.0337)	y	1419.120 (2.060)

Table A2: The basic information for the predicted potential giant magnetocaloric effect candidates ($\Sigma_M > 1.5\%$) in $\text{Fe}_x\text{N}_{1-x}$ ($0 < x < 1$) compounds. The data (in green) of pure α -Fe together with that of (in blue) Fe_3N (#1908) and Fe_4N (#2105) are also listed for comparison.

ID	Com.	ST	SG	ΔE_f	ΔE_H	Σ_M	M_S
2952	Fe_7N	TRI	$P1$	-0.0017	0.0353	9.36	1669.120
7124	Fe_{20}N	TRI	$P\bar{1}$	-0.0042	0.0099	8.85	1803.574
2518	Fe_{19}N	TRI	$P\bar{1}$	-0.0066	0.0082	8.74	1799.372
3110	Fe_{14}N	TRI	$P\bar{1}$	-0.0129	0.0069	8.58	1787.317
4467	Fe_{15}N	TRI	$P\bar{1}$	-0.0095	0.0090	8.57	1788.767
2879	Fe_{16}N	ORT	$Fmmm$	-0.0066	0.0108	8.44	1802.684
2466	Fe_{12}N	TRI	$P\bar{1}$	-0.0192	0.0035	8.44	1778.582
5565	Fe_{13}N	TRI	$P\bar{1}$	-0.0038	0.0173	8.22	1762.738
2226	Fe_{11}N	TRI	$P\bar{1}$	-0.0147	0.0100	8.14	1760.069
1966	Fe_{12}N	MON	$C2/m$	-0.0120	0.0108	8.13	1786.716
3725	Fe_{15}N	MON	$C2/m$	-0.0066	0.0119	8.02	1772.071
510	Fe_8N	TRI	$P\bar{1}$	-0.0031	0.0298	7.79	1714.373
3603	Fe_9N	TRI	$P\bar{1}$	-0.0084	0.0212	7.63	1721.512
4010	Fe_8N	MON	$C2/m$	-0.0218	0.0111	7.56	1747.212
3913	Fe_{11}N	MON	$C2/m$	-0.0110	0.0137	7.34	1750.894
5471	Fe_7N	TRI	$P\bar{1}$	-0.0110	0.0260	7.17	1693.076
1266	Fe_9N	MON	$C2/m$	-0.0157	0.0139	7.13	1732.425
2111	Fe_{16}N_3	TRI	$P\bar{1}$	-0.0004	0.0464	6.65	1603.307
2421	Fe_7N	MON	$C2/m$	-0.0122	0.0248	6.22	1691.750
8109	Fe_8N	TRI	$P1$	-0.0166	0.0163	6.20	1708.572
5266	Fe_6N	MON	$C2/m$	-0.0078	0.0345	5.72	1692.724
617	Fe_5N	MON	$C2/m$	-0.0069	0.0424	5.05	1643.370
6067	Fe_{10}N_3	TRI	$P1$	-0.0080	0.0604	5.02	1395.788
4811	Fe_6N	TRI	$P1$	-0.0144	0.0279	4.84	1615.881
5076	Fe_4N	ORT	$Cmcm$	-0.0073	0.0519	4.69	1548.482
1516	Fe_9N_2	MON	$C2$	-0.0013	0.0526	4.07	1558.602
687	Fe_3N	MON	Pm	-0.0077	0.0663	3.96	1243.857
2958	Fe_{13}N_2	MON	$C2$	-0.0002	0.0393	3.81	1639.209
1609	Fe_5N	MON	$C2$	-0.0077	0.0416	3.42	1573.671
3594	Fe_4N	ORT	$Fmmm$	-0.0040	0.0552	3.37	1619.769
2458	Fe_4N	TRI	$P\bar{1}$	-0.0161	0.0431	3.32	1476.892
7844	Fe_{11}N_3	TRI	$P\bar{1}$	-0.0003	0.0632	3.13	1427.379
1080	Fe_2N	ORT	$Pnmm$	-0.0283	0.0659	2.57	959.379
8255	Fe_9N_2	MON	$C2/m$	-0.0076	0.0462	2.44	1564.765
6365	Fe_7N_3	HEX	$P6_3$	-0.0452	0.0410	2.24	1195.632
2018	Fe_4N	ORT	$Pmma$	-0.0313	0.0279	1.89	1445.983
1546	Fe_3N	ORT	$Immm$	-0.0088	0.0653	1.87	1402.264
1431	Fe_2N	ORT	$Pbcn$	-0.0431	0.0511	1.78	983.927
3566	Fe_4N	ORT	$Pbcn$	-0.0253	0.0339	1.64	1476.661

Table A2 (Continued.)

840	Fe ₃ N	MON	<i>C2/m</i>	-0.0176	0.0564	1.64	1477.306
1617	Fe ₈ N ₃	TRI	<i>P1</i>	-0.0192	0.0604	1.57	1292.213
1	Fe	CUB	<i>Im$\bar{3}m$</i>	0	0	1.57	1784.761
1908	Fe ₃ N	HEX	<i>P6₃22</i>	-0.0740	0	1.93	1419.120
2105	Fe ₄ N	CUB	<i>Pm$\bar{3}m$</i>	-0.0396	0.0196	1.92	1674.060